1.5 μm high detectivity quantum counter by energy transfers in diode pumped glassceramics

F. Auzel, P.A. Santa-Cruz, G.F. de Sá

Classification
Physics Abstracts
78.20 — 78.90 — 78.60 — 81.20Q

1.5 μm high detectivity quantum counter by energy transfers in diode pumped glassceramics

F. Auzel (*), P. A. Santa-Cruz and G. F. de Sá

Dpto de Química Fundamental e Dpto de Física,
UFPE, Cidade Universitária, 50000 Recife PE, Brazil

(*Reçu le 25 juillet 1984, révisé le 15 janvier 1985, accepté le 11 février 1985*)

Résumé. — L'addition de photons par transfert d'énergie (effet APTE) dans des vitrocéramiques dopées Yb^{3+} et Er^{3+} est utilisée pour sommer des photons à 1,5 μm (signal) avec des photons de 0,96 μm (pompe). On discute des différents schémas de transfert d'énergie donnant respectivement le signal somme, les pertes et le bruit afin d'obtenir un compteur quantique infra-rouge (IRQC) de grande détectivité. En optimisant le dopage de la vitrocéramique en même temps que l'intensité du flux de pompage, une puissance équivalente de bruit (NEP) de 10^{-11} W/Hz$^{1/2}$ a été obtenue à température ambiante.

Abstract. — Up-conversion by APTE effect (Addition de Photons par Transferts d'Energie) in (Yb^{3+}, Er^{3+}) doped vitroceramics is used for the summation of 1.5 μm photons (signal) with 0.96 μm (pump). We discuss the different transfers schemes giving respectively the useful signal the losses and the noises in order to obtain a high detectivity IRQC (Infra Red Quantum Counter). Optimizing the vitroceramics preparation as well as the pumping flux intensity, a NEP of 10^{-11} W/Hz$^{1/2}$ has been obtained at room temperature.

1. Introduction.

APTE effect [1, 2] in (Yb^{3+}, Er^{3+}) doped vitroceramics has been found to be a very efficient process to obtain up-conversion by the summation of equal energy photons [3] or of different energy ones [4, 5]. For example, APTE processes have been found to be 10^2 more efficient [2] than sequential absorption which was initially proposed by Bloembergen to obtain IR detection through IRQC process [6].

Sequential absorption in Er^{3+} has already been used as a Bloembergen IRQC at 1.5 μm with diode laser pumping at 0.85 μm and output at 0.55 μm. A Noise Equivalent Power (NEP) of 3×10^{-9} W/Hz$^{1/2}$ was obtained [7].

However due to the low Er^{3+} concentration (0.5 %) no APTE effect was taking place. In this paper we want to discuss how an improve efficiency by APTE effect could affect the NEP of an IRQC. We describe optimized composition materials with vitroceramic structure which provide an IRQC detection of 1.5 μm photons by their APTE summation with 0.96 μm photons produced by a GaAs : Si light emitting diode used as a pump. The sum output signal is obtained at 0.65 μm and can be detected either by a photomultiplier (detection mode) or by a vidicon tube (visualization mode). We shall discuss here the detector mode.

Through an analysis of the different types of energy transfers which contribute respectively to signal, losses and noises, we determine for an optimized composition an optimum of detectivity (NEP) with respect to pumping level.

2. Experimental.

The vitroceramic samples preparation is essentially the same as already described elsewhere [3], except that concentration in active ions (Yb^{3+}, Er^{3+}) were varied in order to optimize a (1.5 μm + 0.96 μm) summation instead of a (0.96 μm + 0.96 μm) one.

Oxides and fluorides of high purity such as Y_2O_3 (99.99 % Molycorp), Er_3O_3 (99.999 % Molycorp), Yb_2O_3 (99.999 % Johnson Matthey), GeO_2 (99.999 % Johnson-Matthey) and PbF_2 (99.99 % Aldrich) were used as starting materials.

Host composition was such that weight ratios of

(*) On leave of absence from : CNET, 196, rue de Paris, 92220 Bagneux, France.

PbF_2 and GeO_2 are :

$$(PbF_2 + GeO_2)/PbF_2 = 1.46$$

and the doping concentrations by weight were :

$$x Er_2O_3 \text{ (with } x = 0.5\,\%;\ 2.0\,\%;\ 5.0\,\%;\ 10\,\%)$$

and

$$y Yb_2O_3 \ (y = 0.5\,\%;\ 7.5\,\%;\ 10\,\%;\ 15\,\%;\ 20\,\%).$$

The starting materials are maintained at 1 000 °C for 1 hour, then poured into a mold at 400 °C and maintained in it for 4 hours. Samples are made of layers of vitroceramics ground to powder of grain diameter $\leqq 200\ \mu$.

The IRQC experimental scheme [8] is given on figure 1. The pump source is a GAL-12 from Plessey with peak emission at $\cong$ 9 400 Å at 25 °C, and spectral half-width of 500 Å. The total emission power is 45 mW at a current of 500 mA. Samples are directly in contact with the diode; the pump is received on one side of the sample, the other side receiving the input signal at 1.5 μm.

The signal source is provided by a tungsten-iodine lamp (150 W) coupled to a dielectric filter centred at 1.54 μm which gives after optical concentration a maximum power density of 10 μW/cm² at the sample. The resulting red output signal is collected from the same side of the sample as the incident 1.5 μm radiation. The output is detected by a Photomultiplier (RCA-C31034) with GaAs photocathode cooled at − 10 °C by Peltier junctions. Between sample and photomultiplier either a multidielectric filter centred at 0.65 μm or a monochromator (Spex Minimate) can be inserted respectively for NEP and intensities and spectral measurements. The output of the photomultiplier is processed by a lock-in amplifier (PAR 124) with plug-in preamplifier (PAR 117) and displayed on a strip chart recorder. The synchronization signal is either derived from the chopper on the 1.5 μ channel or from a pulse generator at the diode input, according to the type of measurement (respectively with or without 1.5 μm photons).

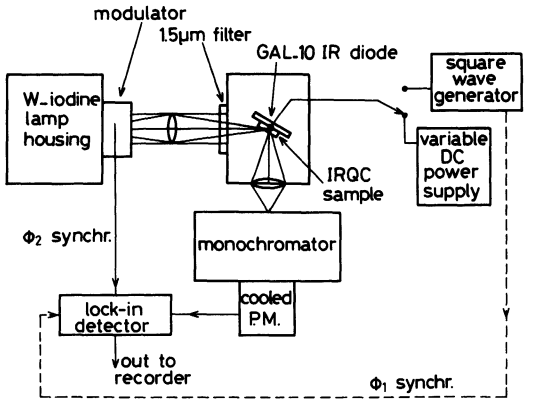

Fig. 1. — IRQC experimental scheme.

As for the excitation spectra, the double beam technique (see Fig. 2) already described in [1] has been used. The sample receives excitation light both from a continuous broad spectral band (0.7 μm-2 μm) beam and from a chopped monochromatic one issued from the same 1 kW tungsten-iodine lamp. A lock-in amplifier processes the signal which occurs for all mono or multi-excitations wavelength combinations giving rise to the red output we are interested in as selected by a 0.65 μm peaked band pass filter.

The diffuse reflectance spectra was obtained with a cary 17 spectrophotometer fitted with its regular double integrating sphere attachment.

3. Experimental results.

3.1 Optimization of concentration of Yb^{3+} and Er^{3+} for maximum sensitivity at 1.5 μm. — For various diode intensity levels at 0.96 μm and constant input signal at 1.5 μm, the curves of figure 3 are obtained. It is found that the output at 0.66 μm varies linearly with pump intensity at 0.96 μm, that the presence of Yb^{3+} does increase the signal output up to a concentration of 10 % and that the best Er^{3+}

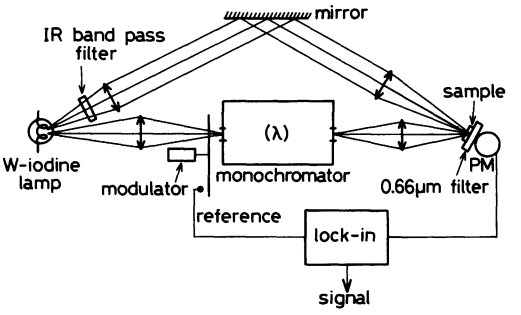

Fig. 2. — Double beam excitation experimental scheme.

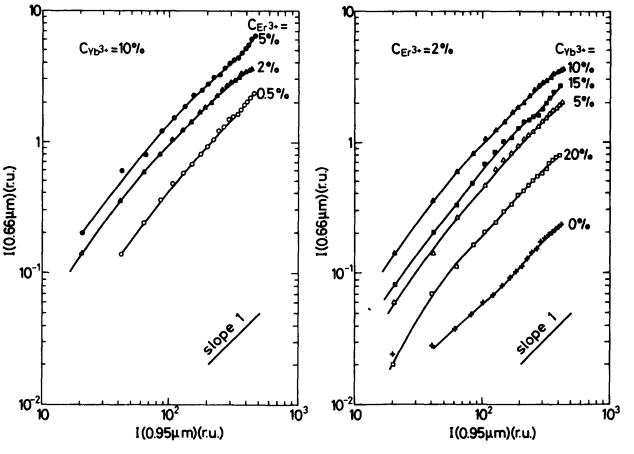

Fig. 3. — Up-conversion emission at 0.66 μm *versus* pump flux (ϕ_1) at 0.96 μm for constant signal (ϕ_2) at 1.5 μm and for different concentrations $C_{Yb^{3+}}$ and $C_{Er^{3+}}$.

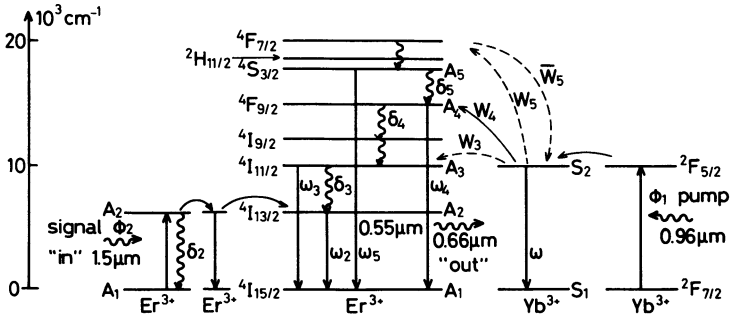

Fig. 4. — Energy levels of Yb^{3+} and Er^{3+} involved in the IRQC scheme.

concentration is 5 %. Concentration are by oxide weight. From the energy level schemes of Er^{3+} and Yb^{3+} and from these results, the excitation process of figure 4 can be derived.

As demonstrated elsewhere [9] for summation of equal energy photons at 1.5 μm in Er^{3+} alone, a first diffusion step is taking place between the first excited states ($^4I_{13/2}$) of several Er^{3+} ions. This explained why a higher concentration of Er^{3+} is required here than for equal photons summation (5 % instead of 2 %) [3]. As well a diffusion process takes place between Yb^{3+} ions up to the point where both diffusions at 1.5 μm and 0.95 μm meet on a common Er^{3+} ion where APTE summation takes place inducing the sequential transitions $^4I_{15/2} \rightarrow {}^4I_{13/2} \rightarrow {}^4F_{9/2}$. This process is quasi-resonant at each step and does not require emission of large number of phonons. It is not the case when $^4F_{9/2}$ emission is obtained by the summation of two or three photons at 0.96 μm [2]. Then the most intense red emission is found for matrices having maximum phonon energy in excess of 500 cm^{-1} [10]. That is mainly for oxidic hosts. Such phonon energy, though enhancing the red emission, is detrimental to the overall efficiency by promoting other non-radiative decays. In the vitroceramics we are dealing with, the Rare-Earths ions segregate preferentially in the fluoride microcrystals [3] the phonon frequency of which can be estimated to be around 350 cm^{-1}. This provides a good overall efficiency when excitation does not imply multiphonon decays or phonon assisted transfer. It is the case for the IRQC scheme of figure 4.

3.2 LOSSY EXCITATION PATHS AND NOISE GENERATION. — In parallel with the IRQC scheme of figure 4, the well known green APTE [2] emission of the Yb^{3+}-Er^{3+} couple can be observed at 0.55 μm when only the pump beam at 0.96 μm is on (see Fig. 4). This constitutes a loss to the detriment of the overall efficiency of the IRQC scheme. On the other hand, as seen on figure 5 some red emission is also produced by the pump alone. This represents a noise for the IRQC scheme of interest. Monitoring both loss

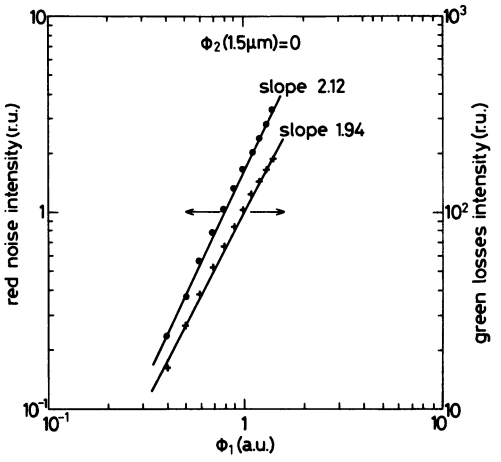

Fig. 5. — Loss (green emission) and noise (red emission) *versus* diode pump flux (ϕ_1) in absence of signal ($\phi_2 = 0$); output signal synchronized on ϕ_1.

(green emission) and noise (red emission) *versus* diode pump flux (ϕ_1) in absence of signal flux (ϕ_2), one obtains for both the quadratic laws shown on figure 5. This type of red emission in Yb-Er systems are known to proceed either by a two-photon or a three-photon process according to the type of host. When some non-radiative decay is allowed the two-photon route is dominant [2]. Though vitroceramics are thought to behave rather like fluoridic hosts [3] rather than oxidic ones, the green to red ratio for 2-photon summation optimized at 2 % of Er^{3+} is known to be a factor 7 instead of 10 for pure fluorides [3].

Then the two-photon process indicated by the quadratic law for red emission on figure 5, can be attributed to some non-radiative leakage either from $^4S_{3/2}$ to $^4F_{9/2}$ or from $^4I_{11/2}$ to $^4I_{13/2}$ following the schemes of figures 6a or b.

As shown farther in section 4, the mechanism of figure 6c which does not involve non-radiative decay, would be a 3-photon process; then it should not be considered here.

Further the optimum Er^{3+} concentration for IRQC at 1.5 μm being larger than for up-conversion of identical photons in the green (5 % *versus* 2 %) due

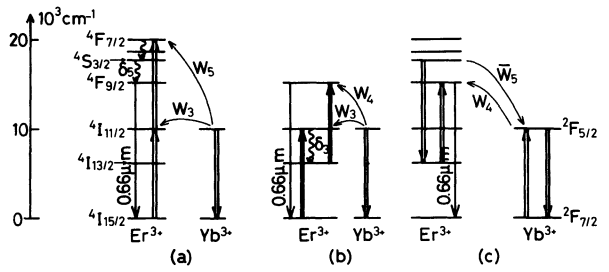

Fig. 6. — Energy schemes for a two-photon red emission contributions : a) by $^4S_{3/2}$ non-radiative leakage; b) by $^4I_{11/2}$ non-radiative leakage and c) for a three-photon red emission contribution without non-radiative decay direct involvement.

to the necessity of diffusion among Er^{3+} ions, has for consequence that some self-quenching of $^4S_{3/2}$ takes place through the following cross-relaxations :

$$Er_A(^4S_{3/2}) + Er_B(^4I_{15/2}) \rightarrow Er_A(^4I_{13/2}) + Er_B(^4I_{9/2})$$

and/or

$$Er_A(^4S_{3/2}) + Er_B(^4I_{15/2}) \rightarrow Er_A(^4I_{9/2}) + Er_B(^4I_{13/2}).$$

Since cross-relaxations of this type populate $^4I_{13/2}$ in absence of signal at 1.5 μm, this population can be recycled as a noise for the IRQC scheme. However a cubic dependence with respect to ϕ_1 should be found for this noise generating process. In any case self-quenching of $^4S_{3/2}$ may exist with a reduction in green emission without efficient recycling as indicated by figure 5, where the green/red ratio is smaller than 7 as expected at lower Er concentration.

From this, the optimum Er^{3+} concentration for IRQC (signal strength) may not be optimum for signal/noise ratio. This point shall be verified by NEP measurements.

Finally a third way to produce red emission without summing 1.5 μm photons with 0.96 μm ones, is obtained by up-conversion at 1.5 μm by three-photon of equal energy summation in Er^{3+} alone by successive excitation of, $^4I_{9/2}$, $^4I_{11/2}$, $^4F_{9/2}$ [9, 11, 12] or enhanced by the cross-relaxation forth and back between Er^{3+} and Yb^{3+} [12] in absence of diode pumping at 0.96 μm. However this red emission depending only on signal source does participate to the signal output and cannot be considered as a noise. Being a higher order process than the one involved in IRQC, it can generally be discarded at the very low input signal (at 1.5 μm) we are interested in.

A typical summation spectrum obtained under both ϕ_2 (1.54 μm) and ϕ_1 (0.96 μm) fluxes is presented on figure 7. ϕ_2 being chopped, the synchronous detector rejects most of the « loss » signal at 0.55 μm (green), whereas emission at 0.812 μm coming from $^4I_{9/2}$ is obtained by non-radiative decay at the expense of $^4F_{9/2}$. For simplification in the discussion (Sect. 4), this last emission is considered together with emission at 0.96 μm from $^4I_{11/2}$.

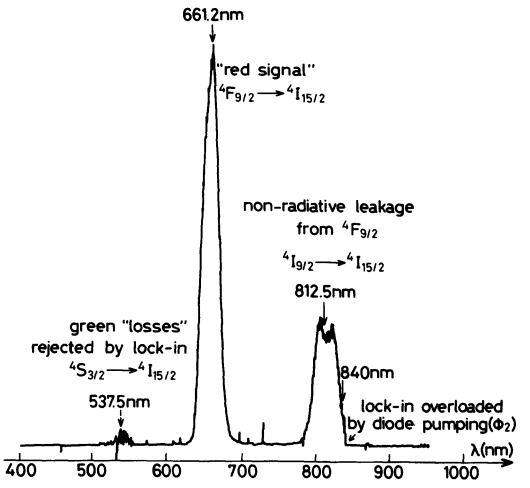

Fig. 7. — Summation spectrum under both chopped ϕ_2 (1.54 μm) and C.W. ϕ_1 (0.96 μm) fluxes. Lock-in detector synchronized on ϕ_2.

3.3 EXCITATION AND DIFFUSE REFLECTANCE SPECTRA. — In order to determine the sensitivity range of the IRQC, the excitation spectra of the up-converted 0.66 μm emission has been obtained as shown on figure 8a by the double beam technique. All contributing wavelength are shown to be essentially arround 1.5 μm and 0.98 μm which correspond to the $^4I_{15/2} \rightarrow {}^4I_{13/2}$ transition of Er^{3+} and $^2F_{7/2} \rightarrow {}^2F_{5/2}$ of Yb^{3+}. The slight excitation arround 1.14 μm corresponds to up-conversion in Er^{3+} alone ($^4I_{15/2} \xrightarrow{1.5\mu} {}^4I_{13/2} \xrightarrow{1.14\mu} {}^4F_{9/2}$) : due to the relatively high Er^{3+} concentration, the first step (1.5 μm) is diffusion enhanced, the second step (1.14 μm) being a direct absorption in Er^{3+}.

The shape of the sensitivity range of the IRQC reflects faithfully the shape of the diffuse reflectance spectra in the same region (Fig. 8). Since the excitation spectra is obtained at low resolution (bandwidth > 200 Å) and the reflectance spectra was obtained with a bandwidth of 50 Å, the absence of particular structure on the sensitivity range is significant. The sensitivity maximum is at 1.52 μm with half sensitivity bandwidth of 750 Å. So the whole band of interest for optical fibers telecommunications around 1.5 μm is covered smoothly.

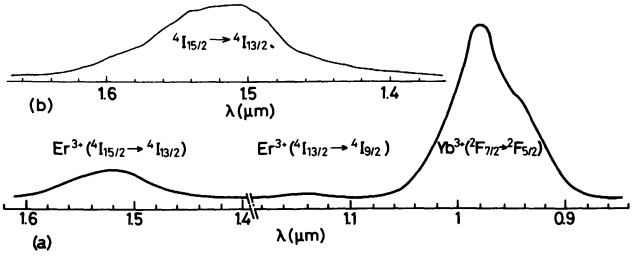

Fig. 8. — Diffuse reflectance spectrum of sample in 1.5 μm region (b) and excitation spectrum for up-conversion of IR to red (0.66 μm) (a).

3.4 NEP MEASUREMENTS. — Sensitivity of a detector can be characterized by its noise equivalent power (NEP) at the input, defined as the minimum detectable signal intensity giving an output signal equal to noise; this being normalized for the used bandwidth which control the amount of noise in the measurement. Two types of measurements are possible; one taken at the output of the photomultiplier, the other at the output of the lock-in.

In both cases, the input signal at 1.5 μm is reduced by a calibrated variable attenuator up to the point where noise intensity (N) is found equal to detected signal (S), figure 9. In the first case S is taken at the output of a relatively large band (MHz) display system (oscilloscope), in the second case at the output of the lock-in with given time constant (RC).

Then NEP $= P_{in}/\sqrt{B}$ for $S = N$ where B is taken equal to the narrowest bandwidth of the considered system. The result should be equal. Differences give some hints about consistency of measurement. In any case the measure with the lock-in is better because more sensitive.

It is this type of measurement generally used [7] that we report here with the lock-in bandwidth given by $B = 1/4\ RC$.

Several measurements at different pump flux intensity (ϕ_1) and Er^{3+}, Yb^{3+} concentration are presented in table I.

4. Discussion.

Since, as shown on figures 3 and 6, both signal and noise increase with pump flux at 0.96 μm, we shall rationalize this situation with rate equations. Our purpose is to understand what the pump conditions should be to obtain a good detectivity. In the following we consider the energy scheme of figure 4 with some simplifying assumptions :

— Diffusion between Er^{3+} and between Yb^{3+} ions are implicitly taken into account by the use of rate equations [13].

— Concentrations $A_1(Er^{3+})$ and $S_1(Yb^{3+})$ are assumed to be smaller than the onset of self-quenching in A and S ions.

— Processes taken explicitly into account are shown on figure 4; their choice is justified by a compromise between intractable complete equations and a practical description of the experimental results of figures 3 and 6.

— Each level emits radiatively principally towards the ground state; non-radiative transitions proceed as usual by steps to next lower state; the largest gap gives the slowest step : for instance, non-radiative transitions from $^4I_{9/2}$ are 150 times stronger than from $^4F_{9/2}$; this allows to lump together populations of several levels : $^4I_{9/2}$ and $^4I_{11/2}$ as A_3 and $^4F_{7/2}$, $^2H_{11/2}$ and $^4S_{3/2}$ as A_5.

The following set of equations is then obtained for the steady state :

$$\frac{dA_2}{dt} = -\omega_2 A_2 - W_4 A_2 S_2 - A_2 \delta_2 + A_3 \delta_3 + \sigma_2 \phi_2 A_1 + \overline{W}_5 A_2 S_1 = 0 \quad (1)$$

$$\frac{dA_3}{dt} = -\omega_3 A_3 + W_3 A_1 S_2 - W_5 A_3 S_2 - A_3 \delta_3 + A_4 \delta_4 = 0 \quad (2)$$

$$\frac{dA_4}{dt} = -\omega_4 A_4 + W_4 A_2 S_2 - A_4 \delta_4 + A_5 \delta_5 = 0 \quad (3)$$

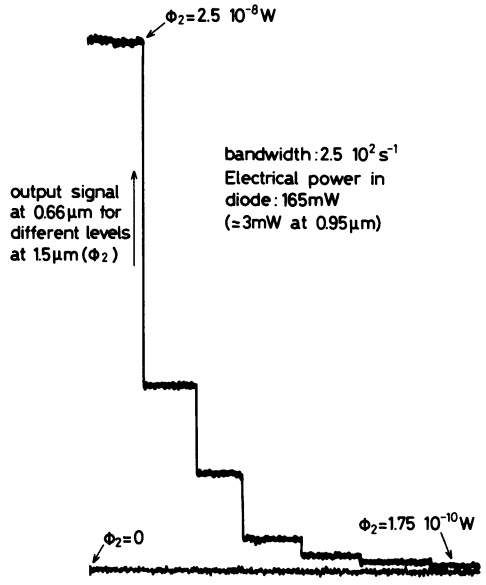

Fig. 9. — Typical signal output for various input power at 1.54 μm (from 2.5 × 10^{-2} μW to 1.7 × 10^{-4} μW on diode size 500 μm × 500 μm) for C_{Er} = 5 %, C_{Yb} = 10 %.

Table I. — *Measured* NEP *values for different* Er^{3+} *concentrations and pump fluxes* ϕ_1 (C_{Yb} = 10 %; RC = 1 ms).

Conditions	NEP (W/Hz$^{1/2}$)		
$C_{Er^{3+}}$ / ϕ_1 elect. power	2 %	5 %	10 %
101 mW	1.3×10^{-11}	6.8×10^{-12}	5×10^{-11}
165 mW	1.9×10^{-11}	1.1×10^{-11}	7.5×10^{-11}
298 mW	6.3×10^{-12}	1.0×10^{-11}	5.5×10^{-11}

$$\frac{dA_5}{dt} = -\omega_5 A_5 + W_5 A_3 S_2 - A_5 \delta_5 - \overline{W}_5 A_5 S_1 = 0 \quad (4)$$

$$\frac{dS_2}{dt} = -\omega S_2 + \sigma_1 \phi_1 S_1 + \overline{W}_5 A_5 S_1 - W_3 S_2 A_1 - W_5 A_3 S_2 - S_2 \delta - W_4 S_2 A_2 = 0 \quad (5)$$

where ω_i are the radiative desexcitation probabilities from level i to ground state; W_i are transfer rate to level i; δ_i are non-radiative decay rate from levels i; populations of ground states $A_1(Er^{3+})$ and $S_1(Yb^{3+})$ are assumed to be practically constant (chemical concentrations), that is only low pumping rates are considered; total decay rates are $\Omega_i = \omega_i + \delta_i$; $\overline{W}_i$ are back-transfer rates; ϕ_1, ϕ_2 are excitation fluxes at 0.96 μm and 1.5 μm; σ_1, σ_2 are absorption cross-sections at these wavelengths.

Involvement of levels higher than $^4F_{7/2}(Er^{3+})$ is known to explain cubic dependence of population on $^4F_{9/2}$ with pumping flux ϕ_1 [2]. Since experimentally a quadratic dependence is found (Fig. 3), we don't consider higher excited states. Recent results have shown [14] that in absence of non-radiative decay, back transfer and cross-relaxation of the type (see Fig. 6c)

$$^4S_{3/2}(Er^{3+}) + {}^2F_{7/2}(Yb^{3+}) \rightarrow {}^4I_{13/2}(Er^{3+}) + {}^2F_{5/2}(Yb^{3+}) \rightarrow {}^4F_{9/2}(Er^{3+}) + {}^2F_{7/2}(Yb^{3+})$$

gives a linear dependence of A_4 *versus* A_5, respectively the population of $^4F_{9/2}$ and $^4S_{3/2}$, $^2H_{11/2}$, $^4F_{7/2}$ lumped together, when $^4F_{7/2}$ is directly excited with visible light. However when IR excited by $Yb^{3+}(S_2)$, a cubic dependence of A_4 on S_2 is found :

$$\omega_4 A_4 \cong \frac{W_3 W_4 \overline{W}_5 W_5 A_1 S_1 S_2^3}{(\omega_3 + W_5 S_2)(\omega_5 + \overline{W}_5 S_1)\omega_2}$$

in absence of saturation ($\omega_2 > W_5 S_2$), though a quadratic one is obtained for A_5 *versus* S_2.

Then the only explanation we are left with to explain the quadratic dependence of A_4 is through non-radiative decays δ_i. This allows us to neglect $\overline{W}_5$ for what we are interested in and to obtain from the equation system :

$$A_2 = \frac{A_3 \delta_3 + \sigma_2 \phi_2 A_1}{(\Omega_2 + W_4 S_2)} \quad (6)$$

$$A_3 = \frac{W_3 A_1 S_2 + A_4 \delta_4}{(\Omega_3 + W_5 S_2)} \quad (7)$$

$$A_4 = \frac{A_5 \delta_5 + W_4 A_2 S_2}{\Omega_4} \quad (8)$$

$$A_5 = \frac{W_5 A_3 S_2}{\Omega_5} \quad (9)$$

$$S_2 = \frac{\sigma_1 \phi_1 S_1}{\Omega + W_3 A_1 + W_4 A_2 + W_5 A_3} \cong \cong \frac{\sigma_1 \phi_1 S_1}{\omega + W_3 A_1} \quad (10)$$

assuming $\delta \ll \omega$ and $A_1 \gg A_2 > A_3$ with W_3, W_4, W_5 of same order of magnitude.

4.1 CALCULATION OF USEFUL SIGNAL AND NOISE TERMS. — The red signal detected by the Photomultiplier (PMT) is given by equation (8) :

$$\omega_4 A_4 = \frac{\omega_4}{\Omega_4}(A_5 \delta_5 + W_4 A_2 S_2)$$

$$\omega_4 A_4 \cong \frac{\omega_4}{\Omega_4}\left[\left(\frac{W_5 W_3 A_1 \delta_5}{\Omega_5 \Omega_3} + \frac{W_4 W_3 A_1 \delta_3}{\Omega_3 \Omega_2}\right) S_2^2 + \frac{W_4 \sigma_2 \phi_2 A_1 S_2}{\Omega_2}\right]$$

$$\cong \frac{\omega_4}{\Omega_4}\left[\frac{W_3 A_1}{\Omega_3}\left(\frac{W_5}{\Omega_5}\delta_5 + \frac{W_4}{\Omega_2}\delta_3\right) S_2^2 + \frac{W_4 \sigma_2 \phi_2 A_1 S_2}{\Omega_2}\right]$$

in which terms in $\delta_i \delta_j$ have been neglected and low pumping fluxes have been assumed.

In absence of signal flux ($\phi_2 = 0$), one obtains the noise terms alone :

$$N = \omega_4 A_{4(\phi_2=0)} = \frac{\omega_4}{\Omega_4}\left[\frac{W_3 A_1}{\Omega_3}\left(\frac{W_5}{\Omega_5}\delta_5 + \frac{W_4}{\Omega_2}\delta_3\right)\frac{\sigma_1^2 \phi_1^2 S_1^2}{(\omega + W_3 A_1)^2}\right] \quad (11)$$

which is found to vary quadratically with pumping flux ϕ_1; it contains two contributions, the first one (δ_5) corresponds to the direct non-radiative leakage from A_5; the second one (δ_3) to the leakage from A_3 recycled as a signal.

The signal term itself is the one depending on ϕ_2 :

$$S = \frac{\omega_4}{\Omega_4} \frac{W_4 \sigma_2 \phi_2 A_1 \sigma_1 \phi_1 S_1}{\Omega_2(\omega + W_3 A_1)} \quad (12)$$

which is found to vary linearly with ϕ_1.

Radiative emission from A_5 does not contribute to noise, however it is a loss to the overall detector efficiency. It is given by :

$$\omega_5 A_5 \cong \frac{\omega_5 W_5 W_3 A_1 S_2^2}{\Omega_5 \Omega_3} = \frac{\omega_5 W_5 W_3 A_1 \sigma_1^2 \phi_1^2 S_1^2}{\Omega_5 \Omega_3(\omega + \omega_3 A_1)} \quad (13)$$

which varies quadratically with flux ϕ_1, of course just as the first contribution to noise which is proportional to it.

So equations (11), (12) and (13) describe well the general behaviour with respect to ϕ_1 as found on figures 3 and 5.

4.2 PUMPING FLUX AND S/N RATIO. — From a detector point of view, we have to investigate the S/N ratio as given by equations (12) and (11).

$$S/N = \frac{\Omega_3}{\Omega_2} \frac{W_4}{W_3} \frac{(\omega + W_3 A_1)}{\left(\frac{W_5}{\Omega_5}\delta_5 + \frac{W_4}{\Omega_2}\delta_3\right) S_1} \frac{\sigma_2 \phi_2}{\sigma_1 \phi_1} \quad (14)$$

which can be further simplified for ease of discussion : taking $\delta_5/\Omega_5 > \delta_3/\Omega_2$, because lifetime of level $^4I_{13/2}$ is usually fifty times larger than the one of $^4S_{3/2}$, then $\Omega_5 \gg \Omega_2$, and $\delta_5 > \delta_3$ because energy gap below $^4S_{3/2}$ is larger than the one below $^4I_{11/2}$, then :

$$S/N \cong \frac{\Omega_3}{\Omega_2} \frac{W_4(\omega/W_3 + A_1)}{(W_5 \delta_5/\Omega_5) S_1} \frac{\sigma_2 \phi_2}{\sigma_1 \phi_1}. \quad (15)$$

It can be identically written :

$$S/N \equiv A \cdot B \cdot C \cdot D \cdot \frac{\phi_2}{\phi_1} \equiv K \frac{\phi_2}{\phi_1} \quad (16)$$

with $A \equiv \Omega_3/\Omega_2$

$B \equiv W_4/(W_5 \delta_5/\Omega_5)$

$C \equiv (\omega/W_3 + A_1)/S_1$

$D \equiv \sigma_2/\sigma_1$.

Besides maximizing each of the above factors, increase in detectivity would seem to impose a pumping flux ϕ_1 as small as possible. Then, reduction in ϕ_1 is only limited by the detectivity of the PMT since the detected signal increases with ϕ_1 ; equation (12) can be identically written :

$$S = \frac{\omega_4}{\Omega_4} \frac{S_1}{(\omega/W_3 + A_1)} \frac{W_4}{W_3} \frac{A_1}{\Omega_2} \times \times \sigma_2 \sigma_1 \phi_2 \phi_1 \equiv k\phi_2 \phi_1 . \quad (17)$$

For a given signal at 1.5 μm (ϕ_2), (16) gives a limitation on ϕ_1 (for $S/N = 1$) as :

$$\phi_1 \leqq K\phi_2 = \phi_{1\,\max} .$$

On the other hand, a given detectivity of the PMT gives the smallest red signal to be detected by it, $S_{\mathrm{PM\,min}}$ as (Eq. (17)) :

$$S_{\mathrm{PMm}} = k\phi_2 \phi_{1\,\min} .$$

In order that a signal ϕ_2 be detected at all, one needs to have : $\phi_{1\,\min} \leqq \phi_{1\,\max}$ (see Fig. 10)

or $$S_{\mathrm{PMm}} \leqq kK\phi_2^2$$

which links the minimum signal $\phi_{2\,\min}$ to be detected by the IRQC detector with given PMT sensitivity limit (S_{PMm}) as :

$$\phi_{2\,\min} = \left(\frac{S_{\mathrm{PMm}}}{kK}\right)^{1/2} \quad (18)$$

$$\phi_{2\,\min} = \frac{\Omega_2}{\sigma_2 W_4}\left(\frac{\Omega_4 W_3 W_5 \delta_5 S_{\mathrm{PMm}}}{\omega_4 \Omega_3 \Omega_5 A_1}\right)^{1/2} \quad (19)$$

Factors in front of square root are more effective on $\phi_{2\,\min}$ variations than factor underneath square root : as a consequence to increase sensitivity (i.e. decrease $\phi_{2\,\min}$) one should primarily decrease Ω_2 (long $^4I_{13/2}$ lifetime); increase σ_2 (absorption cross-section of Er^{3+} at 1.5 μm); increase W_4 (energy transfer to $^4F_{9/2}$). However Ω_2 and σ_2 are not completely independent since $\sigma_2 \propto \omega_2$ and $\Omega_2 = \omega_2 + \delta_2$.

Increasing σ_2/Ω_2 comes out as increasing ω_2/Ω_2 the quantum efficiency of $^4I_{13/2}$ by reducing δ_2 its non-radiative decay. Due to the large energy gap $\Delta E_1 = 6\,600$ cm^{-1} below $^4I_{13/2}$, the corresponding multiphonons non-radiative decay is expected to be small in any oxidic or fluoridic host which does not contain water or radicals with high vibration energy.

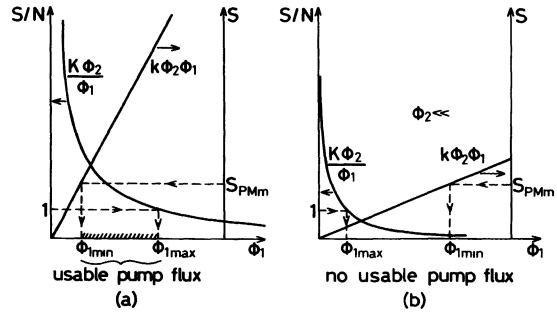

Fig. 10. — S/N ratio evolution with respect ϕ_1 ; role of the PMT sensitivity : a) case where $S/_{\mathrm{PMm}}$ is small enough for given ϕ_2 to have $\phi_{1\,\min} \leqslant \phi_{1\,\max}$; b) case where sensitivity limit of PMT is too large to have $\phi_{1\,\min} \leqslant \phi_{1\,\max}$.

The most likely process reducing $^4I_{13/2}$ efficiency is self-quenching arising for high Er^{3+} concentration (A_1) (between = 6×10^{19} and 6×10^{20} cm^{-3} [15]). Then, provided A_1 is not too large, σ_2/Ω_2 is not likely to vary much from host to host.

Increasing W_4 comes out as maximizing multiphonon energy transfer :

$$^4I_{13/2}(Er^{3+}) + {}^2F_{5/2}(Yb^{3+}) \rightarrow {}^4F_{9/2}(Er^{3+}) + {}^2F_{7/2}(Yb^{3+}) + 1\,200\ \text{cm}^{-1}(\Delta E_2).$$

Due to the large ratio $\Delta E_1/\Delta E_2 \cong 5.5$ and the exponential variation of multiphonon processes with energy gap, this can be readily compromized with a good $^4I_{13/2}$ efficiency.

At this point we have to consider terms underneath square-root because in rare-earth system vibronic properties of host effect all electronic levels simultaneously according to the energy gap involved in the multiphonon process; further it can generally be assumed that vibronic properties vary more from host to host than electronic ones.

Then one should secondarily increase the quantum efficiency of $^4F_{9/2}(\omega_4/\Omega_4)$; decrease transfer rate to $^4I_{11/2}$ and $^4S_{3/2}$ (W_3 and W_5); reduce non radiative transitions (δ_5); reduce the lifetimes of $^4I_{11/2}$ and $^4S_{3/2}$; increase Er^{3+} concentration (A_1); reduce the NEP of the used PMT (S_{PMm}).

Among those factors only, S_{PMm} is evidently independent of others. However because W_3 and W_5 characterize nearly resonant transfer, they can be considered host independent. A_1 can be increased up to the point of self-quenching of $^4I_{13/2}$.

We are left with minimizing :

$$\frac{\Omega_4}{\omega_4}\,\frac{\delta_5}{W_4^2}$$

where $\dfrac{\Omega_4}{\omega_4} = 1 + \dfrac{\delta_4}{\omega_4}$ and where δ_4 implies for the slower step a multiphonon gap $\Delta E_4 \approx 2\,400$ cm^{-1} (between $^4F_{9/2}$ and $^4I_{9/2}$); δ_5 implies $\Delta E_3 \cong 2\,500$ cm^{-1} (between $^4S_{3/2}$ and $^4F_{9/2}$); W_4 implies $\Delta E_2 \cong 1\,200$ cm^{-1}.

Because of $\Delta E_4 \cong \Delta E_3$ and of the constant part in Ω_4/ω_4 we consider essentially δ_5/W_4^2

$$\frac{\delta_5}{W_4^2} = \frac{\delta_5(0)\exp - \alpha\,\Delta E_3}{W_4^2(0)\exp - 2\,\beta\,\Delta E_2}$$

where $\delta_5(0)$ and $W_4(0)$ characterize electronic parts of the multiphonon processes; α and β are respectively the exponential multiphonon parameter for non-radiative decay and energy transfers [15]. Since $\beta \cong \dfrac{\alpha}{2}$ [16]

$$\frac{\delta_5}{W_4^2} \cong ct \times \exp - \alpha(\Delta E_3 - \Delta E_2) \cong \cong ct \times \exp - 1\,300\,\alpha.$$

Comparing different host gives for this factor :

	α[17]	$(\exp - 1\,300\,\alpha)^{1/2}$
oxide	3×10^{-3} cm	1.4×10^{-1}
fluoride	5×10^{-3} cm	3.8×10^{-2}
chloride	11×10^{-3} cm	7.8×10^{-4}

Assuming for vitroceramics a fluoride behaviour, an increase by a factor 50 could readily be obtained for NEP using an anhydrous chloride matrix.

NEP results in table I can be understood in the following way : increasing A_1 from 2 % to 5 % increases sensitivity as shown by a reduction in NEP at smaller ϕ_1 (101 mW) as predicted by equation (19). From 5 % to 10 % this improvement effect is counterbalanced by a reduction in σ_2/Ω_2 due to $^4I_{13/2}$ self-quenching taking place in that range [15].

As predicted by equation (16) (for $S/N = 1$), increasing ϕ_1 decreases sensitivity by increasing NEP. However above $\phi_1 = 165$ mW a decrease in NEP is experimentally observed which cannot be understood within the considered model unless saturation in « green loss » generation be taken into account as due to saturation in $^4I_{11/2}$ population. The fact that this effect is stronger for the smallest A_1 concentration (2 %) is an indication for such effect.

5. Conclusion.

APTE effect in Yb^{3+}-Er^{3+} doped vitroceramics has been shown to produce a high detectivity IR quantum counter with NEP $\cong 10^{-11}$ W/$\sqrt{\text{Hz}}$ at 1.54 μm, a wavelength region used for third generation optical fiber communications.

Simple rate equations approach has conducted to a study of the behaviour of S/N ratio with respect to pumping flux, radiative and non-radiative probabilities as well as activator concentration. Due to its simplicity, its built in ruggedness, its sensitivity and its relatively low response speed ($\cong 10^{-3}$ s), encompassed applications could be found in simple visualization devices for « on field » testing of futur optical fiber systems.

Acknowledgments.

Its a pleasure to thank Mlle D. Morin from CNET (Bagneux) for advice in sample preparation, Mlle S. Hubert from IN2P3 (Orsay) for obtaining IR excitation spectrum, and Pr. O. L. Malta (UFPE) for helpful discussions. Financial assistance from CNPq is gratefully acknowledged.

References

[1] AUZEL, F., *C. R. Hebd. Séan. Acad. Sci.* (Paris) **263** (1966) 819.

[2] AUZEL, F., *Proc. IEEE* **61** (1973) 758.

[3] AUZEL, F., PECILE, D., MORIN, D., *J. Electrochem. Soc.* **122** (1975) 101.

[4] MITA, Y., *Appl. Phys. Lett.* **39(B)** (1981) 587.

[5] AUZEL, F., DE AZEVEDO, W., DE SA, G. F., Proc. Inter. Conf. on lasers and Applications, 10-15 September 1982 Bucharest.

[6] BLOEMBERGEN, N., *Phys. Rev. Lett.* **2** (1959) 84.

[7] STOKOWSKI, S. E., *J. Appl. Phys.* **45** (1974) 2957.

[8] SANTA-CRUZ, P. A., AZEVEDO, W. M., DE SA, G. F., *Nova Q.* **6** (1983) 149.

[9] AUZEL, F., Proceedings of ICL'84 Madison, Wisconsin, to be published by North Holland.

[10] MATSUBARA, T., *Jpn J. Appl. Phys.* **11** (1972) 1579.

[11] JOHNSON, L. F., GUGGENHEIM, H. J., RICH, T. C. and OSTERMAYER, F. W., *J. Appl. Phys.* **43** (1972).

[12] ARAPOVA, E. Y., ZAMKOVETS, N. V., SIBELDIN, N. N., TIMOFEEV, Y. P. and FRIDMAN, S. A., *Opt. Spectrosc.* **40** (1976) 172.

[13] AUZEL, F., in *Radiationless Processes* ed. B. Di Bartolo and V. Goldberg (Plenum) 1980, p. 252.

[14] STAPOR, A., Proceedings XII Conference on Physics of semiconducting compounds, Yascoviec, Poland, 1983.

[15] AUZEL, F., *Ann. Telecommun.* **24** (1969) 199.

[16] MIYAKAWA, T. and DEXTER, D. L., *Phys. Rev.* **B 1** (1970) 2961.

[17] AUZEL, F., in *Luminescence of Inorganic Solids* ed. B. Di Bartolo (Plenum) 1978, p. 71, 107.